



DOI: 10.18720/MCE.90.10

Ductility and moment redistribution capacity of two-span RC beams

R. Ehsani, M.K. Sharbatdar*, A. Kheyroddin

Semnan University, Semnan, Iran

**E-mail: msharbatdar@semnan.ac.ir*

Keywords: high performance fiber reinforced cement composites, two span concrete beam, ductility, moment redistribution, steel fibers

Abstract. The particular weaknesses of concrete buildings are brittle fracture and lack of material ductility, so using steel reinforcements and discrete fibers are an attempt to overcome this weakness. Strain hardening behavior under tensile force has made new material, High Performance Fiber Reinforced Cement Composite “HPFRCC” as a high performance material with high energy absorption capability and high cracking ability before failure. Therefore the structural application of this composite material in the structural members such as continuous beams to control cracks width and formation of multiple cracks, improve ductility, moment redistribution capacity have been investigated. In this paper, the effect of using HPFRCC containing 2 % steel fibers on the flexural performance of four large two-span reinforced concrete beams with similar dimensions and similar longitudinal reinforcement ratios has experimentally been investigated. Two beams were ordinary concrete with two different arrangements of stirrups in the middle support (hogging) and mid span (sagging) area and two other beams were companion but made with full HPFRCC composites. The specimens have rectangular cross section of 250 mm (height)×200 mm (width) and are continuous over two spans of 1800 mm each and two concentrated equal statically monotonic loads (from zero to the failure) are applied at the mid-span of each beam. The experimental results showed that using HPFRCC layers in section beams and reducing the spacing of the stirrups, increased the ultimate load, ductility ratio, plastic hinge characteristics and moment redistribution capacity of these beams compare to reference beam. The greatest load carrying capacity values 42 % were observed in FHPS compared to RCN beam. Maximum moment redistribution values of around 23.31 % was observed in FHPS beam and maximum displacement ductility ratio 1.8 was observed in FHPS beam compare to reference beam. In HPFRCC beam, the sufficient shear strength is provided in beam without local shear cracks. This allows the formation of plastic hinge in beams and plastic hinge zone.

1. Introduction

One of the high performance materials that has been prominent in recent years is the high performance fiber reinforced cement composites (HPFRCC). Strength, stiffness, toughness (the area under the stress-strain curve) and durability are the main characteristics of a High Performance Material. researchers investigated Durability of an Ultra High Performance Fiber Reinforced Concrete (UHPRFC) [1]. HPFRCC were classified in a way, which was separated from fiber reinforced Concrete (FRC), so HPFRCC were a special type of FRC composites whose characteristic sign was the strain hardening behavior under tensile force after the first cracking, which was accompanied by multiple cracks to reach high strains [2]. Researcher have recently looked at the applications of high performance fiber- reinforced cement composites [3]. At present, the most widely used micro and nanomodifiers of cement composites and simultaneously components of the cement stone are the finely dispersed active mineral additives such as silica foam and metakaolin [4–8]. It is known that concrete is a heterogeneous material, it has the low tensile strength to compressive strength ratio, and is prone to formation of microcracks in the process of shrinkage during hardening. These peculiarities determine the necessity of the solution of specific problems to identify the optimal combination of the

Ehsani, R., Sharbatdar, M.K., Kheyroddin, A. Ductility and moment redistribution capacity of two-span RC beams. Magazine of Civil Engineering. 2019. 90(6). Pp. 104–118. DOI: 10.18720/MCE.90.10

Эхсани Р., Шарбатдар М.К., Хайруллин А. Пластичность и способность перераспределения моментов двухпролётных железобетонных балок // Инженерно-строительный журнал. 2019. № 6(90). С. 104–118. DOI: 10.18720/MCE.90.10



This open access article is licensed under CC BY 4.0 (<https://creativecommons.org/licenses/by/4.0/>)

concrete matrix with different types of reinforcing fibers which technical characteristics may be varied within wide limits. The use of a fiber reinforcement allows to improve the tensile strength and tensile strength in bending, impact and fatigue strength, reduce the shrinkage the deformations, prevent the cracking, increase the flexibility, impact, and abrasive resistance, increase frost resistance, water resistance, etc. By applying the disperse reinforcing fibers of different types and sizes, we can adjust characteristics of concrete thereby ensuring required performance properties and durability [8–12].

Many structural applications of HPFRCC material are concentrated on simple beams, continuous beams (moment redistribution as effective parameters in RC structures), and beam-column connections, so the related researches are given following. Hemmati et al. (2015), performed experimental parametric studies to evaluate the impact of compressive strength, loading type and tensile reinforcement ratio on the characteristics of the final deformation of simplified support beams HPFRCC. It showed that, if concentrated loading in the middle of the span were changed to uniform loading, the plastic hinge rotation capacity would increase and examined the flexural behavior of high performance fiber reinforced concrete beams with the effect of the thickness of the HPFRCC layer at the height of the beam's cross section under a two-point flexural test also Researcher conducted research on increasing the bearing capacity in reinforced concrete frame using HPFRCC materials by numerical methods. In these models, the panel zone material was replaced by HPFRCC, which had different tensile and compressive strengths, and then complete concrete frames and complete HPFRCC frame were compared. The results showed that the use of these materials increased the bearing capacity and ductility of these frames [13–16].

Maghsoudi et al. (2010), investigated of reinforced high strength concrete continuous beams strengthened with fiber reinforced polymer. Experimental program was focused on flexural behavior and moment redistribution in continuous HSC beams. It was concluded that, as the number of CFRP sheet layers increases, the ultimate strength becomes higher, but the ductility, moment redistribution and ultimate strain of the CFRP sheet decrease. An analytical model for moment–curvature and load capacity were developed and used for the tested specimens. Good agreement between experiment and prediction values was reported [17].

And also Carmo et al. (2008) studied analytically factors affecting moment redistribution in continuous RC structures which are ignored in design codes. The studied parameters are structural type, load type, concrete strength, and beam slenderness. The main objective of the study was to understand better the capacity of forces redistribution in reinforced concrete beams [18–21]. Moreover, Holschemacher et al. (2012) investigated continuous two-layer reinforced concrete beam. 5 Models and full-scale statically determinate two-layer beams (TLB), made of steel fiber high strength concrete (SFHSC) in the compression zone and normal strength concrete (NSC) in the tensile zone, have been tested by the Researchers. As in the previous research stages, interaction of the concrete layers in a CTLB was studied to demonstrate the efficiency of such beams for real structures. No cracks between the SFHSC and NSC layers were observed up to the ultimate limit state of the tested beam, which demonstrates proper interaction between the layers. The results obtained in the present study enable a recommendation of CTLB for practical application as effective and economical continuous bending elements [23–25].

Mostofinejad et al. (2007) conducted a parametric study on moment redistribution in continuous RC beams with equal spans under uniform loading was performed. First, the governing equation for the allowable percent of moment redistribution was extracted using ductility demand and ductility capacity concepts. The effects of different parameters such as the concrete compressive strength, the amount and the strength of reinforcing steel, the magnitude of elastic moment at the support and the ratio of the length to the effective depth of the continuous beam on moment redistribution were then investigated. The results showed that, whereas the permissible moment redistribution in continuous reinforced concrete beams based on the relevant rules in the current codes is not in a safe margin in some cases, it is rather conservative in most cases [26]. Visintin et al (2018) investigated the moment redistribution in ultra-high performance fiber reinforced concrete beams. The results of the experimental investigation show that for beams where the hinge formed at the support, the observed moment redistribution was greater than the code predictions. However for the beam where the hinge formed under the load points, observed moment redistribution was significantly less than codes predictions. Hence, the results of this study show current design guidelines do not always provide a conservative prediction of moment redistribution in UHPFRC beams [27].

Bagge et al (2014) investigated the moment redistribution in RC beams, study of the influence of longitudinal and transverse reinforcement ratios and concrete strength. Evaluation of the experimental study indicated a highly nonlinear structural behavior of the tested beams with the distribution of moment differing from linear elastic analysis, even for low load levels. The evolution of moment redistribution and the moment redistribution at the ultimate limit state (ULS) were appreciably dependent on the arrangement of longitudinal reinforcement, whilst the transverse reinforcement ratio had a marginal impact up to yielding of the longitudinal reinforcing steel, with the concrete strength slightly reducing the degree of moment redistribution [28, 29].

Saghafi et al. (2018) investigated enhancement of seismic performance of beam-column joint connections using high performance fiber reinforced cementitious composites. The test results revealed that HPFRCC connections considerably enhanced shear and flexural capacity as well as deformation and damage

tolerance behavior at post-cracking stage compared to those of normal concrete at ultimate stages. Moreover, the failure mode of HPFRCC specimens changed from shear mode to flexural mode compared to the failure mode of concretes without required seismic details [30, 31].

A survey of literature shows that more experimental work is needed to investigate the use of HPFRCC material instead of normal concrete in continuous concrete beams and a research program must be established for investigating the structural behavior of a RC beam with HPFRCC. A great amount of researches in recent years, focused on the durability and steel corrosion of these composite beams and it is necessary to evaluate the structural behavior of these hybrid members. Furthermore, very limited research studied the effect of HPFRCC and confinement of concrete in compression on the rotational capacity, ductility and the capacity of redistributing stresses and moments between positive and negative regions of reinforced continuous concrete beams.

This paper examines the complete nonlinear response of a RC continuous beam and HPFRCC continuous concrete beams tested under monotonically increasing loads. From a different perspective, an important issue in designing HPFRCC continuous beams is the requirement of appropriate ductility and the capacity of redistributing stresses and moments between positive and negative regions. Given the collapsing flexural modes in these beams, the analysis of stress and moment redistribution calls for special investigation.

2. Methods

2.1. Materials properties of experimental program

In this research, the components of the materials and the mixing design used for constructing High Performance Fiber Reinforced Cement Composite (HPFRCC) were result of testing the specimens with different proportions of materials to achieve hardening behavior. So that the best mixing design based on Weight ratio was presented in Table 1. The cement amount used in the construction of beams was Portland cement with density of 3.05 g/cm^3 and the sand used in HPFRCC concrete had a diameter of 0.1 mm to 2.4 mm. In the construction of Normal Strength Concrete (NSC). Aggregates with a maximum diameter of 10 mm were used and the sand was smaller than 4.75 mm (sieve number 4). Sand and gravel had a specific density of 2.65 g/cm^3 . Silica fume with density of 2.2 g/cm^3 and grain size $0.1 \mu\text{m}$ and super plasticizer based poly-carboxylate with a density of about 1.07 g/cm^3 were used in the construction of concrete beams. Hook-end steel fibers with 30 mm length, 0.6 mm diameter, aspect ratio (l/d) of 50, tensile strength 1100 MPa, modulus of elasticity 200 GPa and density 7.85 gm/cm^3 were employed in this study. The density of this steel fiber is 7850 kg/m^3 and the weight of 0.01 m^3 of this fiber is 7850, so the volume fraction equal 2 % means that from 100 percentage of total volume of each cubic meter of concrete, 2 % equal 0.02 m^3 and 157 kg filled with steel fiber.

Table 1. Mixture proportions of HPFRCC and NSC.

Name of material	Concrete Components							
	Cement (Kg/m ³)	Sand (kg/m ³)	Gravel (kg/m ³ *)	Water (kg/m ³)	Super plasticizer (kg/m ³)	Silica fume (kg/m ³)	Steel fiber (kg/m ³)	Fiber volume fraction V_f (%)
HPFRCC*	850	1062	–	257	13.77	85	157	2
NSC**	450	597	1083	210	–	–	–	–

* High performance fiber reinforced cement Composite, ** normal strength concrete

Six cube samples with dimensions of $150 \times 150 \times 150 \text{ mm}$ were used to determine the compressive strength of normal strength concrete (NSC) and HPFRCC. The mean values of the 28 day compressive strengths of cubic samples for NSC and HPFRCC were 42.62 and 82.94 MPa, which were equal to 36.22 and 70.50 MPa in compressive strength cylindrical samples, respectively. The typical setup for the uniaxial tensile test is shown in Figure 1. To avoid fractures outside the measurement area, both ends of the specimens were made in the shape of a dog-bone. The elongation of the specimen was measured using two linear variable displacement transducers placed on two opposite sides of the specimen with a gauge length of 100 mm. The load was applied using displacement control hydraulic jack at a constant rate of 0.1 mm/min. Tensile Stress-strain responses of specimens was shown in Figure 1. The measured stress-strain curves are presented in Figure 1. The maximum tensile strain exceeded 0.71 % and the maximum tensile strength was approximately 6.7 MPa.

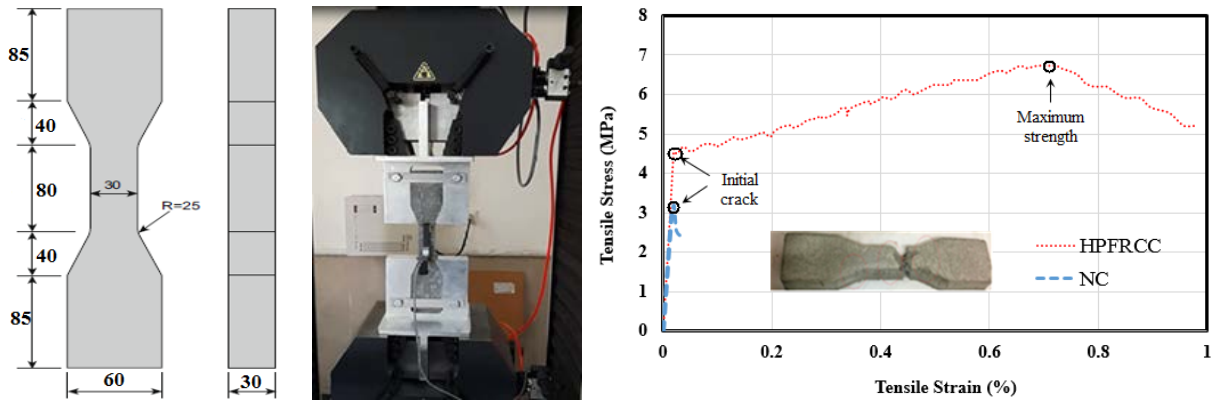


Figure 1. Dog-bone specimen configuration for uniaxial tensile tests (Units: mm).

In Table 2. Some important characteristics associated with the reinforcing steel are shown for all dimensions used for reinforcing the beams. The yield strength (f_y), yielding strain (ϵ_{sy}), ultimate strength (f_u) and ultimate strain (ϵ_{su}) are presented as mean values from standardized material tests.

Table 2. Reinforcing steel characteristics.

Type of rebar	Diameter Φ (mm)	Yielding strength f_y (MPa)	Yielding strain ϵ_{sy} (%)	Ultimate strength f_u (MPa)	Ultimate strain ϵ_{su} (%)	Modulus of elasticity E_s (MPa)
Longitudinal rebar	14	520	0.25	640	16	210
Longitudinal rebar	10	530	0.24	663	16	210
Transverse rebar	8	510	0.20	780	14	210

2.2. Test setup and instrumentation

In order to study the flexural behavior of two-span continuous beams with conventional concrete and HPFRCC composite, specimens had been selected that were as close to half-scale as possible to achieve reliable results. The general test set-up was shown in Figures 2 and 3, the beams consisted of two equal spans with two roller supports at both ends and one hinged support at the middle. A 1000 kN hydraulic actuator was used to apply a monotonic concentrated load on the mid-point of a rigid steel spreader beam. And also three load cells were used to measure the reaction at the supports. To measure the applied total load by hydraulic jack, a Load cell with a capacity of 1000 kN was used. Moreover, deflection was measured, using Linear Variable Differential Transformers (LVDTs), at three different locations in each span: at the midpoint, one-quarter, and three-quarters of the span length. Considering the distance of the experimental rigid frames and considering this limitation, the beams were 4000 mm long with two equal spans (1800 mm each span) to which two concentrated forces were applied at mid span. The beams were rectangular 250 mm \times 200 mm (height \times width) and this cross section was constant in all tests, as was the slenderness, $L/h = 7.2$ (L is the span length and h is the beam height) as shown in Figure 4.

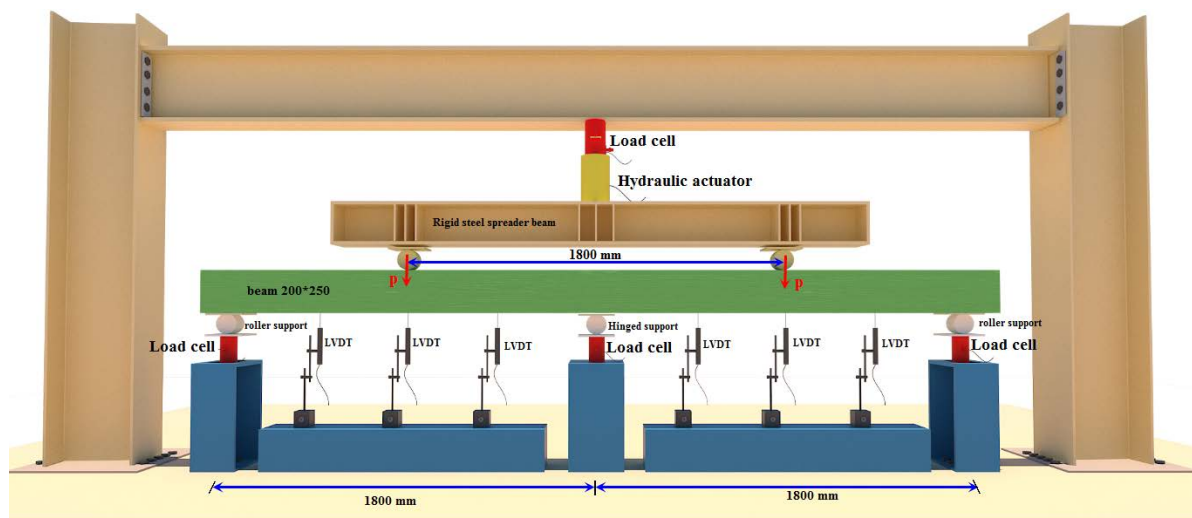


Figure 2. Test setup and instruments used in experiment of the beams.



Figure 3. General view of the test setup.

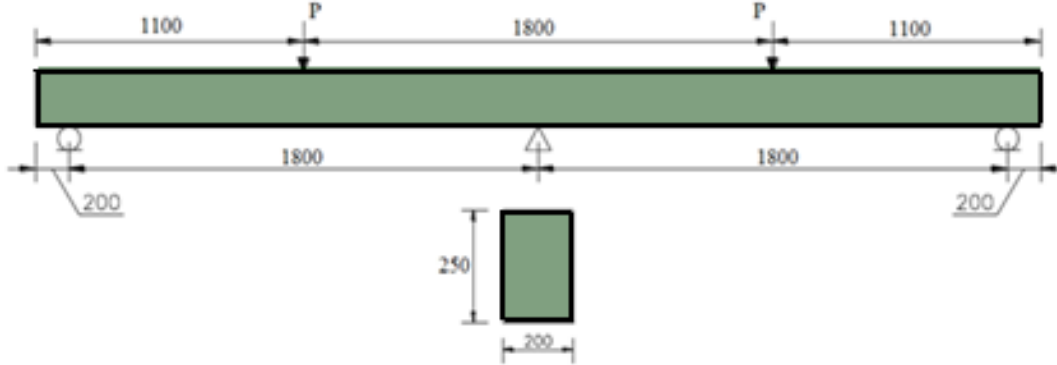


Figure 4. General Dimension of test specimens (unit: mm).

The reinforcement ratio (ρ_1, ρ_2) consumed in these beams was selected in such a way that the area section of bars was not more than balance reinforcement ratio (ρ_b) so the flexural failure occurred, this assumption was shown in Figure 5. As shown in Figure 6, two and three bars of 14 mm in diameter were used as the bottom and top longitudinal reinforcement negative moment at middle support and two bars of 14 mm in diameter as top and three bars of 14 mm and one bar of 10 mm were used at the maximum positive moment in the middle of the span. At the middle support section, the reinforcement ratio (ρ_1) was 0.01 and at mid-span section (ρ_2) was 0.012. This means that the longitudinal reinforcement ratio the mid – span section was 1.2 times that at the middle support section to allow plastic moment redistribution. In addition, the ratio of the bars used was more than Minimum amount and brittle failure did not occur in specimens. The area of the Stirrups used in these experimental samples was chosen in a way that was more than the minimum shear reinforcement. Therefore, the shear failure in these beams did not occur and the flexural behavior was dominant. After cracking of critical sections in a continuous steel-reinforced concrete beam, the difference between actual and predicted linear- elastic moment distribution in such beams can be identified in two stages. The first stage is caused by difference in concrete cracking in critical regions, and the second stage is caused by plastic deformation of steel reinforcement. Also, for beams with constant cross-section, flexural stiffness after cracking was found to be approximately proportional to tensile reinforcement ratio. Consequently, the distribution of bending moment after cracking will change according to the provided reinforcement as demonstrated in Figure 5. Electrical Strain Gauges (ESG) with a length of 30 mm and the electrical resistance of 120 ± 0.3 ohms were attached to the reinforcement and concrete surface at the three critical locations: middle support and two mid-span sections, as shown in Figures 6-a and 6-b. The details of all specimens are given in Table 3.

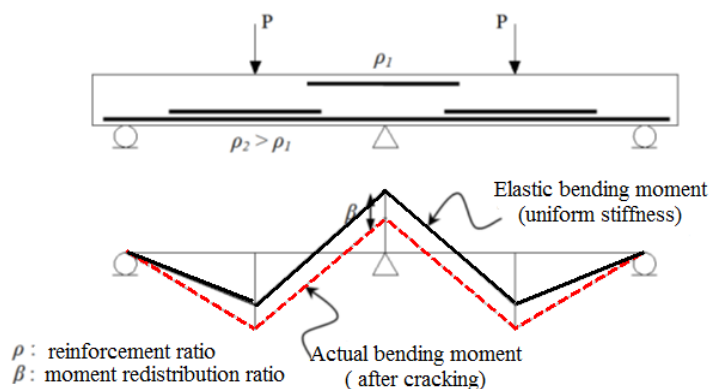


Figure 5. Elastic and actual bending moment in a continuous beam.

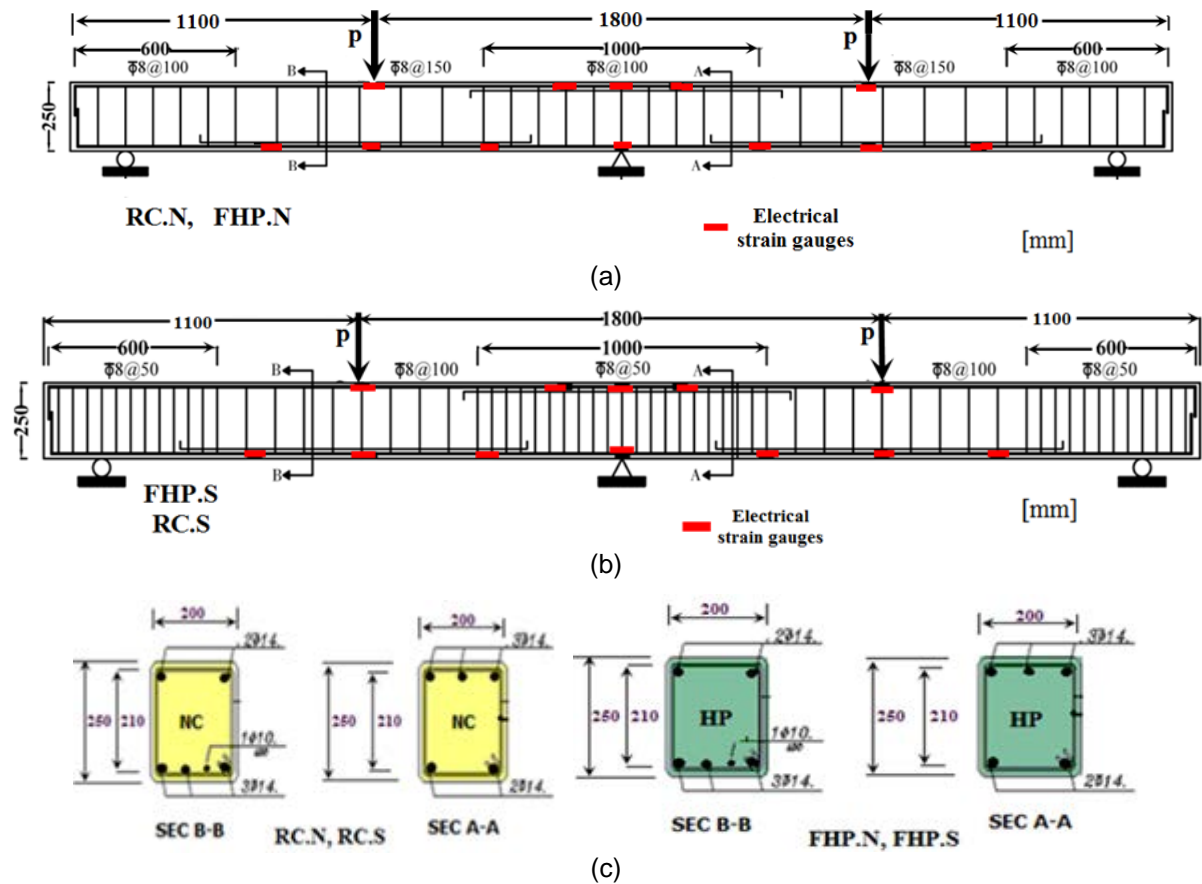


Figure 6. Reinforcement details of the beams: a) Reinforcement arrangement, FHP.N and RC.N Specimens. b) Reinforcement arrangement, FHP.S and RC.S Specimens. c) Typical Cross sections of beams in sagging (M^+) and hogging (M^-) region.

Table 3. Reinforcement Details and Concrete Properties of Tested Beam.

Specimen name	Cross section $b \times h$ (mm)	(NSC) and (HPFRCC) Compressive strength (MPa)	(NSC) and (HPFRCC) tensile strength (MPa)	Longitudinal bars at positive moment (M)	Longitudinal bars at negative moment (M^+)	Stirrups at the supports	Transverse reinforcement ratio (ρ_v) at the supports (%)	Stirrups in the middle of the span	Transverse reinforcement ratio (ρ_v) at middle of the span (%)
RCN*	200x250	36.22	3.44	3Ø14+1Ø10 (540.35)	3Ø14(462) mm ²	Ø8@100	0.5	Ø8@150	0.33
RCS**	200x250	36.22	3.44	3Ø14+1Ø10 (540.35) mm ²	3Ø14(462) mm ²	Ø8@50	1	Ø8@100	0.5
FHPN***	200x250	70.50	6.90	3Ø14+1Ø10 (540.35) mm ²	3Ø14(462) mm ²	Ø8@100	0.5	Ø8@150	0.33
FHPS****	200x250	70.50	6.90	3Ø14+1Ø10 (540.35) mm ²	3Ø14(462) mm ²	Ø8@50	1	Ø8@100	0.5

* Reinforced Concrete and Normal spacing stirrups, ** Reinforced concrete and special spacing stirrups, *** Reinforced HPFRCC and normal spacing stirrups, **** Reinforced HPFRCC and special spacing stirrups.

The stirrups and reinforcement ratios are accordance with the provision of American Concrete Institute [32], therefore the amount of transverse reinforcement was variable in this experimental study. Two beams, RC.S and FHP.S, were provided with transverse reinforcement ratio ($\rho_v = A_v / bs$) equal 2 higher than beams RC.N and FHP.N at the supports and approximately 1.5 higher than beams RC.N and FHP.N at middle of span. A bar of 8 mm was used, which its center-to-center distance was 100 mm. In addition, in the middle of the span and at a distance of 50 mm in the shear area, a bar of 8 mm was used, which its center-to-center distance was 150 mm. In non-closed space samples, in the middle of the span, bars of 8 mm were used, which its center-to-center distance was 150 mm and in the shear area its distance was about 100mm in order to set stirrups. Before loading the beams, all strain gauges were installed and the load cell performed completely during loading.

3. Results and Discussion

Mode of failure, load-deflection, load-strain, moment and load capacity, moment redistribution and ductility are the obtained results to be presented and discussed in following sections.

3.1. Failure mode and general behavior

Generally, the experimental results showed that the initiation and propagation of cracks in beams were depended on the tensile strength of the concrete mix, and the type of the reinforcement. Moreover the first cracks were vertical flexural at the middle support section followed by similar vertical cracks at mid-span, good agreement with the elastic bending moment distribution in continuous beams resulting in higher moment at middle support compared with that at mid span. Therefore the cracking pattern of specimens RCN and RC.S was similar that the first cracks in these two beams were in the negative moment region at the internal support. By increasing load, the new vertical and diagonal flexural cracks were observed in the positive and negative moment regions of both spans. The number of cracks at the middle support in beams with smaller stirrup spacing was more than those beams with wider spacing, the stirrups act as crack initiator and affect the flexural crack spacing and longitudinal reinforcement ratio at critical sections was effective factor to control the width of flexural cracks [31].

3.2. Load-deflection response and failure mode

The ultimate loads measured by the load cells of specimens are given in Table 4 and the load- deflection (in the middle of each span) curves of all the tested beams are shown in Figure 7. Ultimate load and corresponding vertical deflection of beam RCN were respectively 163.70 kN and 50.71 mm and these amounts for RCS with more transverse reinforcement were 186.94 kN and 79.00 mm. The ultimate loads of HPFRCC beams FHPN and FHPS were 205.63 kN and 229.88 kN, and their corresponding deflections were 83.27 mm and 98.66 mm, respectively.

Table. 4. Load and displacement of the tested beams.

Specimen notation	At Cracking		At yielding		At ultimate		$\frac{P_u}{P_{u(RC.N)}}$	Failure mode
	P_{cr} (kN)	Δ_{cr} (mm)	P_y (kN)	Δ_y (mm)	P_u	Δ_u		
RCN	31.25	1.76	147.48	11.28	161.85	50.71	1.0	Concrete crushing, Longitudinal steel bars rupture
RCS	35.93	1.63	160.21	14.27	186.94	78.99	1.15	Longitudinal steel bars rupture
FHPN	41.32	1.52	184.15	12.19	205.63	93.63	1.27	Longitudinal steel bars rupture
FHPS	46.27	1.41	198.73	12.84	229.88	104	1.42	Longitudinal steel bars rupture

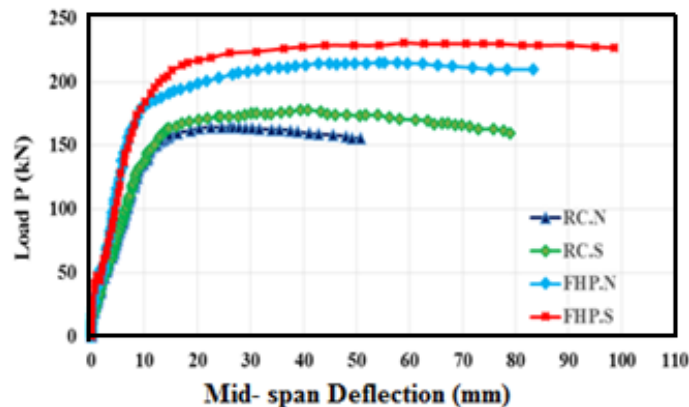


Figure 7. Load-deflection relationships for tested beams.

A comparison of the cracking load, yielding load, ultimate load, and corresponding deflection, and for all samples was shown in Figure 8. Further increase in cracking load in FHPS and FHPN beams compared to RCN and RCS beams was due to the hardening effects of HPFRCC composites. This could also be cited for yielding load, and maximum loads in beams, which were made with HPFRCC composite. Moreover, the beams constructed with closed space stirrups in comparison to beams with non-closed space stirrups showed an increase in cracking load, yielding load and maximum loads due to reducing and limiting the width of the crack and the non-extension of the shear and flexural cracking. Increased load was considerable in the beams made with HPFRCC composite. In the case of observed cracks in HPFRCC composite beams, it could be concluded that the fibers in the tensile section of these beams could control the width of the cracks and create more cracks. On the other hand, the force drop in these beams was lower than that of conventional concrete beams, so the HPFRCC composite beams exhibited a more ductile behavior. Considering the operability and ensuring the satisfaction of service of the flexural member, the generated deformation in the beams under the working

load would be ranging from $\frac{l}{480}$ to $\frac{l}{180}$ (3.75 mm to 10 mm for the mentioned beams) in accordance with

the allowable value according to the ACI 318M-08, depending on the type and function of the structure. According to the results of the experiments, the deformations generated in the load operation were in the satisfactory range of codes.

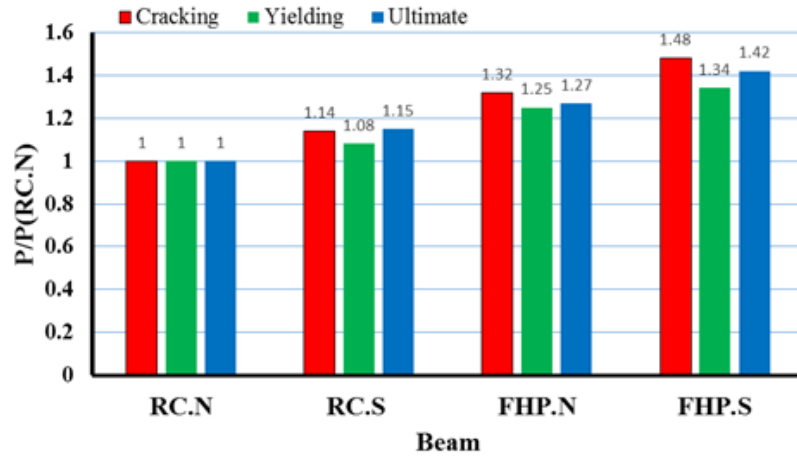


Figure 8. Comparison of loads ratio in cracking, yielding and ultimate modes.

The tested beams behavior before cracking was linear load-deflection. Upon cracking, stiffness was reduced as the load increased. Control beam, RCN, The tensile steel yielded ($P_y = 147.48$ kN) prior to concrete crushing at both the central support ($P_u = 161.85$ kN) and mid-span section as shown in Figure 9a. The new wider flexural cracks were occurred at the mid-span and center support and extended to the compressive regions. The tensile steels at central support of beam RCS were yielded at a load of 160.21 kN and the beam failed over the central support at the load 186.94 kN shown in Figure 9-b. The yielding loads of beams FHPN and FHPS were 184.15 and 198.73 kN prior to concrete crushing at both the center support and mid – span section as shown in Figures 9c and d. The beam failed by tensile rupture of the reinforcing bars prior to concrete crushing at both the central support and mid-span section as shown in Figure 9c. All beams exhibited three stage responses up to failure: representing the concrete pre cracking stage. Concrete post cracking to tension steel pre yield stage, tension steel post yield stage to failure.

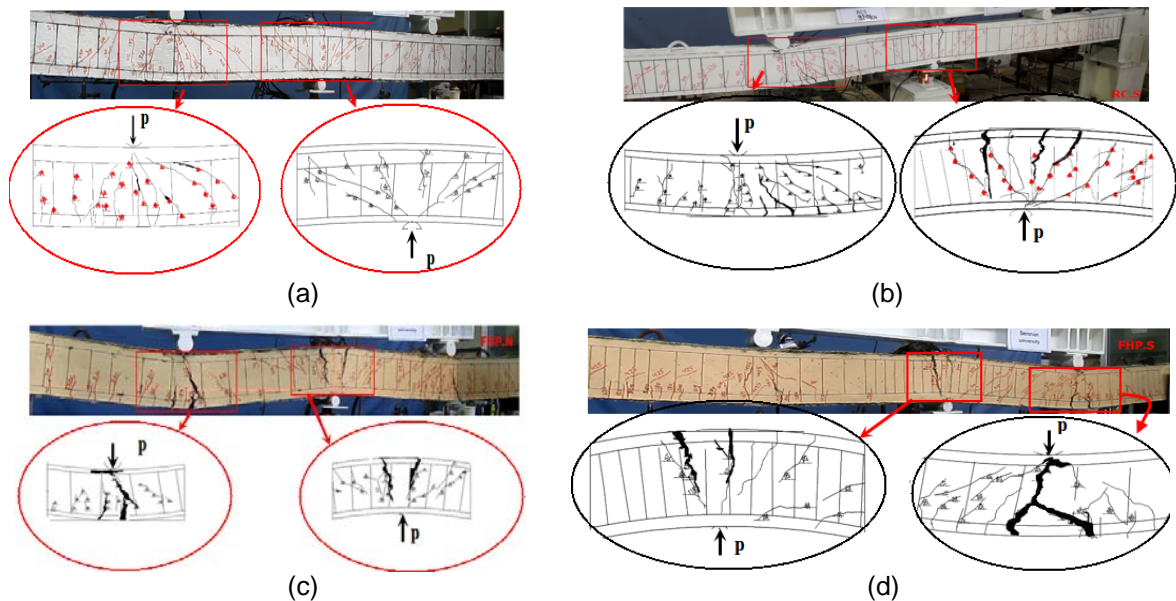


Figure 9. Failure shape and cracking pattern of tested beams: (a) RCN, (b) RCS, (C) FHPN, (d) FHPS.

Increasing the transvers reinforcement, as in beams RC.S compared with RC.N, resulted in improved ultimate load capacity and less deflection at any particular applied load. The transverse reinforcement ratio (ρ_v) of beam RC.S was twice of that of beam RC.N at the supports, resulting in 15 % increase in the ultimate load and 8 % reduction in mid-span deflection. Comparison of load-displacement curves of FHPN and FHPS beams in Figure 7 shows that the ultimate load capacity of specimen with closer stirrup spacing was improved and also its mid-span deflection was reduced. Therefore this issue had a positive effect on rotation capacity and moment redistribution at critical sections.

By observing the load-displacement response curves, it was shown that the FHPS and FHPN beams were ductile and the absorption capacity of energy had improved considerably and dramatically. The ultimate load in the FHPS sample increased by 42 % and the ductility coefficient of displacement was 80 % higher than RCN sample. By comparing the failure modes in Figure 9, the load-displacement response curve showed that FHPN and FHPS and RCS samples exhibited more ductile behavior than RCN samples, the first cracks started in the tested beams from the central support. When the load was applied to the beams, at the beginning of the loading, the severity of the load was low, the structure behaved as a linear elastic and the structure response was linear

and it was proportional to the load applied. At the critical zone (central support), when the load reached to P_{cr} , the hardness decreased in the cross section, so elastic re-distribution occurred, i.e. the critical section (central support) transferred some moment to the sections that had not yet been cracked (mid-span). In FHPFRCC beams with closed space shear reinforcement, crack width was less than RCN. The reason was the reinforcing effect of HPFRCC in preventing the expanding of cracks. In addition, by comparing the load – displacement response of the samples in Figure 7 and the presented results in Table 4, it could be seen that in the beams containing HPFRCC, the resistance against cracking and initial hardness of the samples had been increased. The increase in cracking load in HPFRCC samples, compared to RCN, was attributed to the role of HPFRCC composites in limiting the expansion of the cracks.

3.3. Ductility

The ductility of a beam can be defined as its ability to sustain inelastic deformation without loss of its load carrying capacity prior to failure. Ductility is more important for statically indeterminate structures, such as continuous beams, as it allows for moment redistribution through the rotation of plastic hinges. Ductility has generally been measured by a ratio called the ductility index or factor (μ). The ductility index is usually expressed as a ratio of rotation (θ), curvature (ϕ), deflection (Δ), and absorbed energy (E) at failure (peak load) divided by the corresponding property when the steel starts yielding. The displacement ductility index is defined by Equation

$\mu_{\Delta} = \frac{\Delta_u}{\Delta_y}$. Where Δ_u is the mid-span deflection at ultimate beam load and Δ_y is the mid-span deflection at

yielding load of the tensile steel reinforcement at the central support. The mid-span deflection at beam ultimate load (Δ_u) and yielding load (Δ_y), and the deflection ductility index (μ_{Δ}) are given in Table 5. As can be seen from Table 5, increasing the transverse reinforcement and closer stirrup spacing, in beams RCS and FHPS compared with RCN and FHPN resulted in improved displacement ductility. Comparing RCN with FHPN and RCS with FHPS, it can be seen that using HPFRCC allowed for more displacement ductility in the ultimate failure load beams. Figure 10 shows this positive effect on available rotation capacity and moment redistribution at critical sections. Another way of defining ductility was based on the concept of energy. Therefore, the energy density index μ_E , was the ratio of the absorbed energy of the beam of the ultimate load to the absorbed energy at the

yielding load. The quantity of energy was defined as $\mu_E = \frac{E_u}{E_y}$, in which, the energy absorbed by the E_u was

the beam in the ultimate load and E_y was the energy absorbed in the yielding load. In the present study, ductility was obtained based on displacement and absorbed energy methods. The energy density index μ_E are given in Table 5. As can be seen from Table 5, increasing the transverse reinforcement and closer and smaller spacing stirrup spacing, in beams RC.S and FHP.S compared with RC.N and FHP.N resulted in increased in energy density index (μ_E). Comparing RCN with FHPN and RCS with FHPS in Figure 11, it can be seen that using HPFRCC resulted in increasing in energy density index (μ_E).

Table 5. Energy and displacement ductility of the beams.

Specimen	$\mu_{\Delta} = \frac{\Delta_u}{\Delta_y}$	$\frac{\mu}{\mu_{(RC.N)}}$	E_y (kN.mm)	E_u (kN.mm)	$\mu_E = \frac{E_u}{E_y}$	$\frac{\mu_e}{\mu_e(RC.N)}$
RCN	4.5	1.0	737	7137	10	1
RCS	5.5	1.2	801	8921	11.1	1.2
FHPN	7.7	1.7	822	10706	13	1.3
FHPS	8.1	1.8	920	13454	14.6	1.5

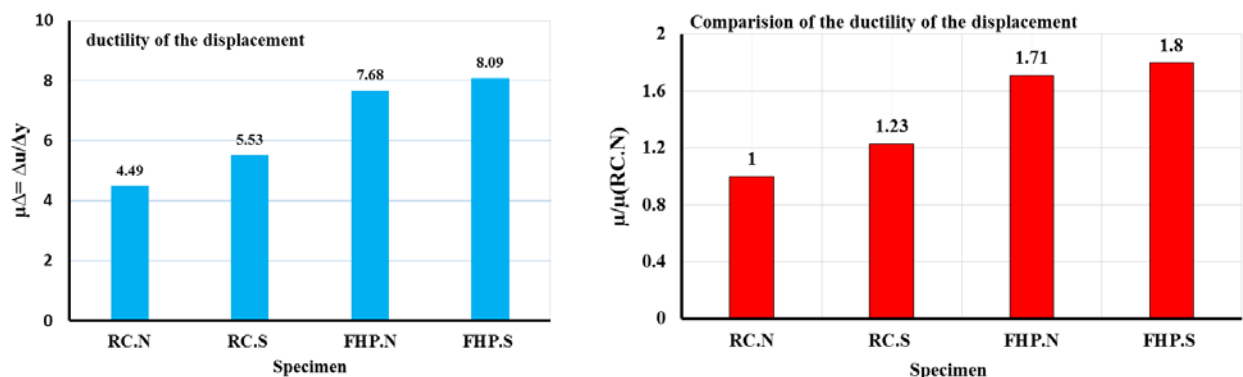


Figure 10. Displacement ductility of specimens.

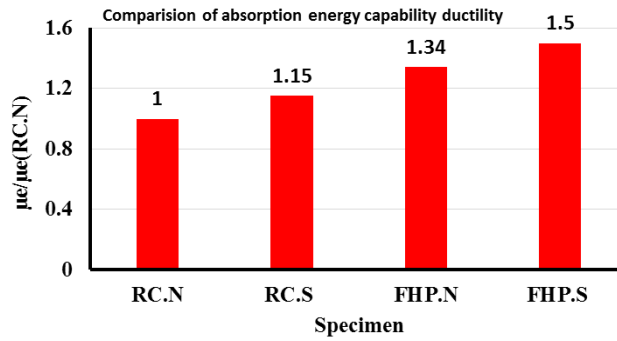
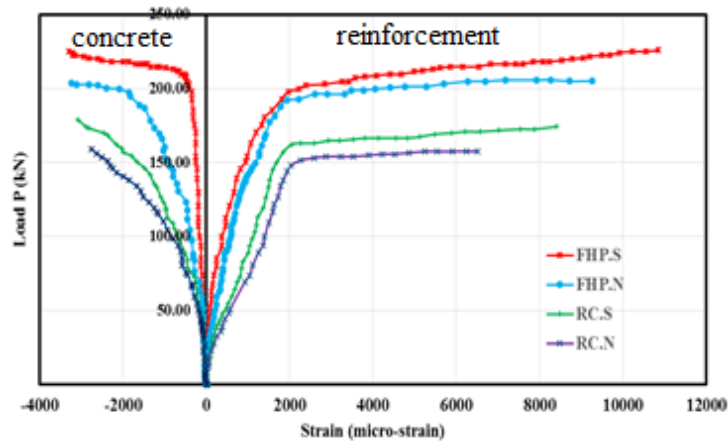


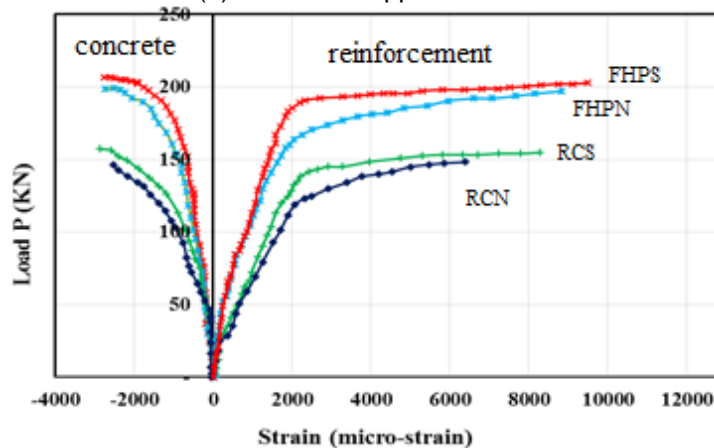
Figure 11. Energy ductility of specimens.

3.4. Load-strain response

The maximum measured strains of steel bars and concrete at the critical sections (mid-span and middle support) against the applied load are shown in Figure 12, indicating that the compressive strains in concrete at failure reached or exceeded the maximum compressive strain of 0.003. The section at middle support in all tested beams were cracked prior to the mid-span section. The measured strains in the top reinforcement over the middle support was about 1.2 times that in the bottom reinforcement at mid-span in all reinforced beams. In the FHPS sample, due to the greater confinement effect of closed- space stirrups, as well as the strain hardening effect on HPRCC, and because the fibers had maintained integrity, they could tolerate larger deformations and reinforcement had experienced larger strains. In the RCN beam under increasing loading, the cracks expanded faster and pressure concrete was crushed. Therefore, due to damage of the compressive concrete, the balance of the conventional reinforced concrete section collapsed and the applied force was falling down. Thus, the ductility of the NSC beams was less than that of the HPRCC beams.



(a) At middle support section



(b) At mid-span section

Figure 12. Load-strain curves.

3.4. Moments – curvature in critical section

Experimental moment – curvature response at sagging and hogging sections for tested beams are shown in Figure 13. The forces applied to the mid-span of the beams and the supports were measured by the load cell to calculate the moment at critical sections. The tensile strain values of the tensile reinforcements, which were also used to calculate the curvature of the beam, measured by the strain gauge connected to the

tensile reinforcement in the critical sections. The curvature at central support or mid – span is calculated by dividing the concrete strain ε_c by a distance to the neutral axis depth, c and given as $\varphi = \frac{\varepsilon_c}{c}$. In Figure 13a, it was clear that the ultimate moment value for the RCN beam was 45.78 kN.m. For example, ultimate moment value for RC.S, FHP.N and FHP.S were 51.57, 55.20 and 59.65 kN.m, respectively. The greatest increase in flexural strength in the central support of the FHP.S sample was found to be about 1.30 times more than the RC.N sample. According to Figure 13b, the ultimate moment capacity in the mid-span for the RC.N sample was 50.84 kN.m, while for RCS, FHPN and FHP.S samples, it was 58.33, 64.93 and 73.62 kN.m, respectively. The greatest increase in flexural capacity was observed in the mid-span of the FHP.S sample, which was about 1.44 times more than the RCN sample.

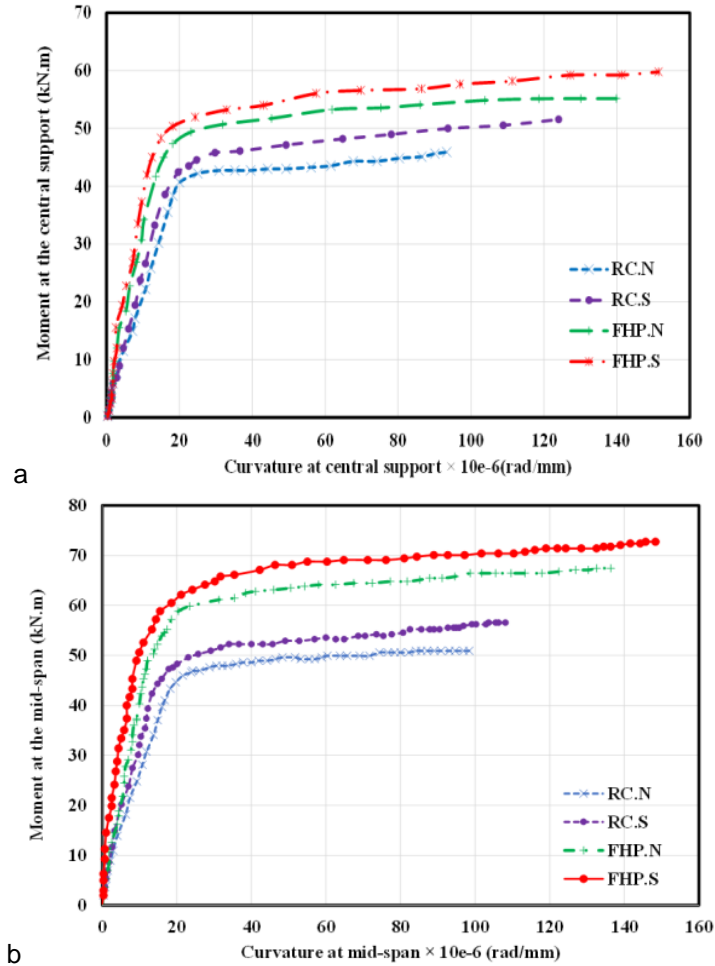


Figure 13. Moment-Curvature: a) at the central support b) at the mid-span.

In the Table 6, a summary of flexural capacity in the mid-span and central support for the specimens was recorded, as well as the increase of the flexural capacity in the critical sections for RC.S, FHP.N and FHP.S beams were compared with the RC.N beam. In this table, M_m^+ and M_C^- were respectively the positive moments in the central support and the negative moment in central support of the beams. In addition, φ_u and φ_y , respectively, were curvature in the ultimate state and curvature in the yielding state of the sections.

$\left(\frac{\varphi_u}{\varphi_y}\right)_m$, $\left(\frac{\varphi_u}{\varphi_y}\right)_c$ were the curvature ductility factor in the central support and mid-span.

Table 6. Flexural strength of samples in the central support and mid-span, and the ratio of increasing flexural strength and curvature ductility factor of beams.

Beams	M_C^- (kN.m)	M_m^+ (kN.m)	$\frac{M_C^-}{M_{C(RC.N)}}$	$\frac{M_m^+}{M_{M(RC.N)}}$	$\left(\frac{\varphi_u}{\varphi_y}\right)_c$	$\left(\frac{\varphi_u}{\varphi_y}\right)_m$
RC.N	45.78	50.84	1.00	1.00	4.75	4.72
RC.S	51.57	58.33	1.12	1.14	5.54	5.50
FHP.N	55.20	64.93	1.20	1.27	6.27	6.20
FHP.S	59.65	73.62	1.30	1.44	6.59	6.50

3.5. Moment redistribution

Since beams were statically indeterminate, the calculation of actual internal forces were based on the measured reactions. The variation of reactions versus the applied load for all tested beams are shown in Figure 14. The elastic end reaction with the value $R_1 = 0.312P$ and the elastic central support reaction with the value $R_2 = 1.376P$ was also plotted to evaluated the amount of load redistribution. Where R_1 and R_2 are the end and middle support reaction respectively. As shown in Figure 14, at the beginning of loading, the reaction force of the central and lateral support was similar to that obtained by linear analysis. In loads greater than the yielding load of tensile steel, at the same load level, the experimental reactions at the lateral supports were greater than the calculated reaction of the elastic relations. The experimental bending moments at both the middle support and mid-span were calculated using the measured reactions. The amount of moment redistribution can be obtained by comparing the actual and elastic bending moment. Diagrams of moment-load were also shown in the positive area (mid-span) and the negative (central support) for the tested beams in Figure 15. The moment in the mid-span and central support was calculated from the static equation and also based on the reaction of the center and lateral supports. As shown in Figure 15, in loads greater than the yielding load of tensile load, at the same load level, the moments in the central supports and the mid-span (under load) were less and more than the moments calculated from the elastic relations, respectively. The diagrams for moment were shown in both ultimate elastic and experimental modes for the tested beams in Figure 15. As shown in Figure 7, in the ultimate load, the difference between the experimental and elastic moment was due to moment redistribution. The amount redistribution ratio (β) given in Table 7 was calculated for the sagging and the hogging bending moment at mid-span and at the central support at failure load. The ratio was calculated by $\beta = \frac{M_e - M_{exp}}{M_e} \times 100\%$, which

M_{exp} is the actual moment at an applied load; and M_e is elastic moment corresponding to the applied load. As indicated in Table 9, beam RCN had a moment redistribution ratio of 16.42 % at central support and 9.9 % at mid-span. The moment redistribution ratio of RCS, FHPN and FHPS beams was significantly increased due to smaller spacing stirrup and HPFRCC in beams. Actual versus elastic bending moment curves at failure are shown in Figure 16.

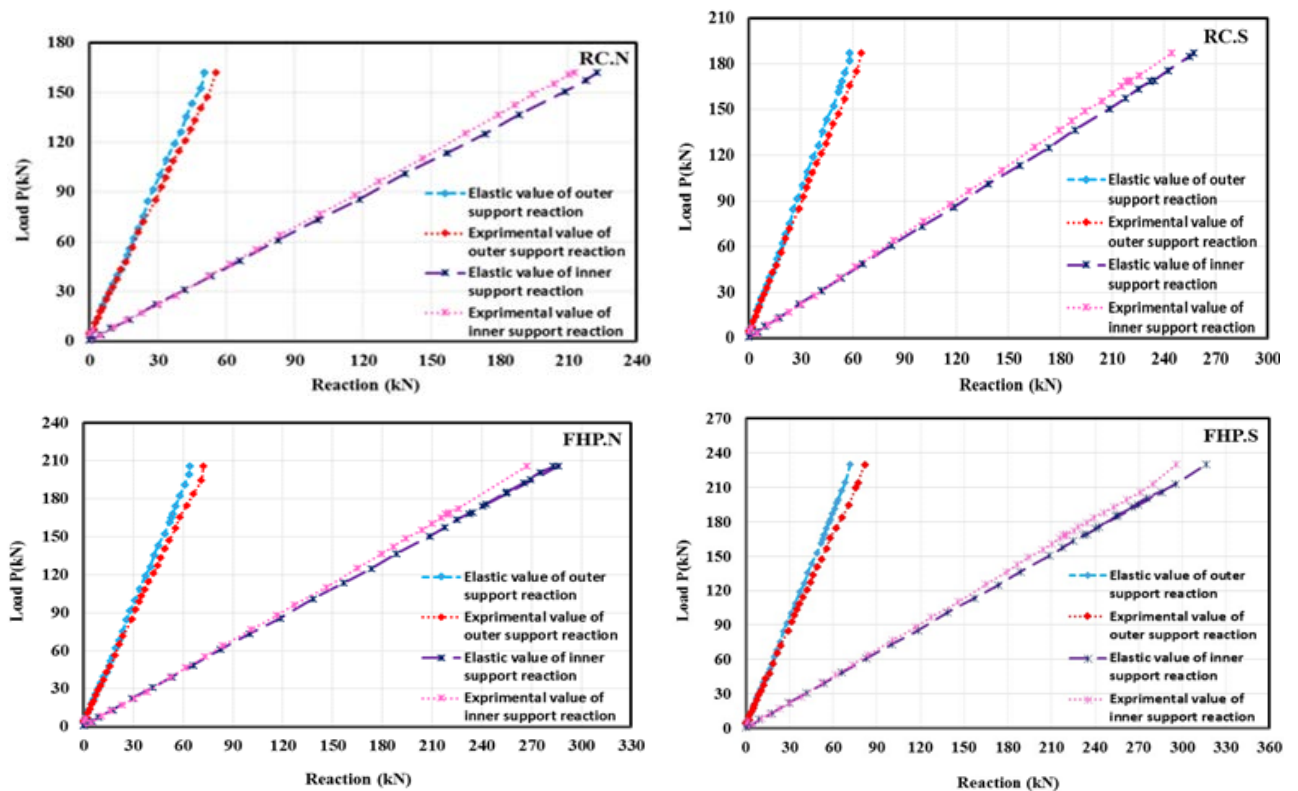


Figure 14. Load versus end and central support reactions of the tested beams.

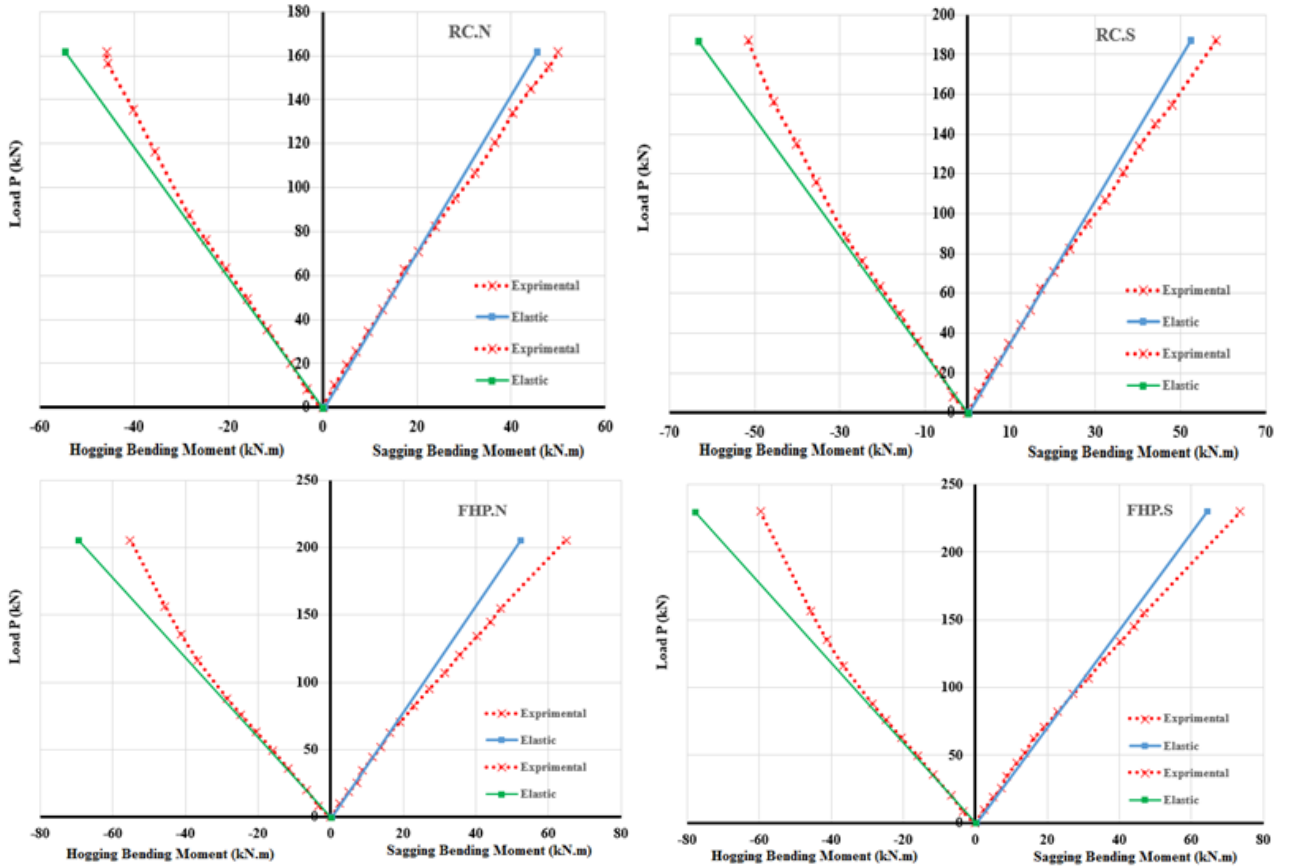


Figure 15. Applied load versus bending moment of tested beams.

Table 7. The amount of the reaction force of the lateral support, central support, the moment, and moment redistribution of the tested beams.

Beam	Ultimate load P_U (kN)	Reaction force of lateral support (kN)	Reaction force of central support (kN)	Central support			Mid-span		
				Elastic moment (kN.m)	Experimental moment (kN.m)	%MR β	Elastic moment (kN.m)	Experimental moment (kN.m)	%MR β
RC.N	161.85	55.49	212.72	54.78	45.78	16.42	45.44	49.94	-9.9
RC.S	186.94	64.82	244.24	63.27	51.57	18.49	52.49	58.33	-11.12
FHP.N	205.63	72.15	266.96	69.59	55.20	20.67	59.88	64.93	-12.47
FHP.S	229.88	81.80	296.16	77.79	59.65	23.31	64.54	73.62	-14.06

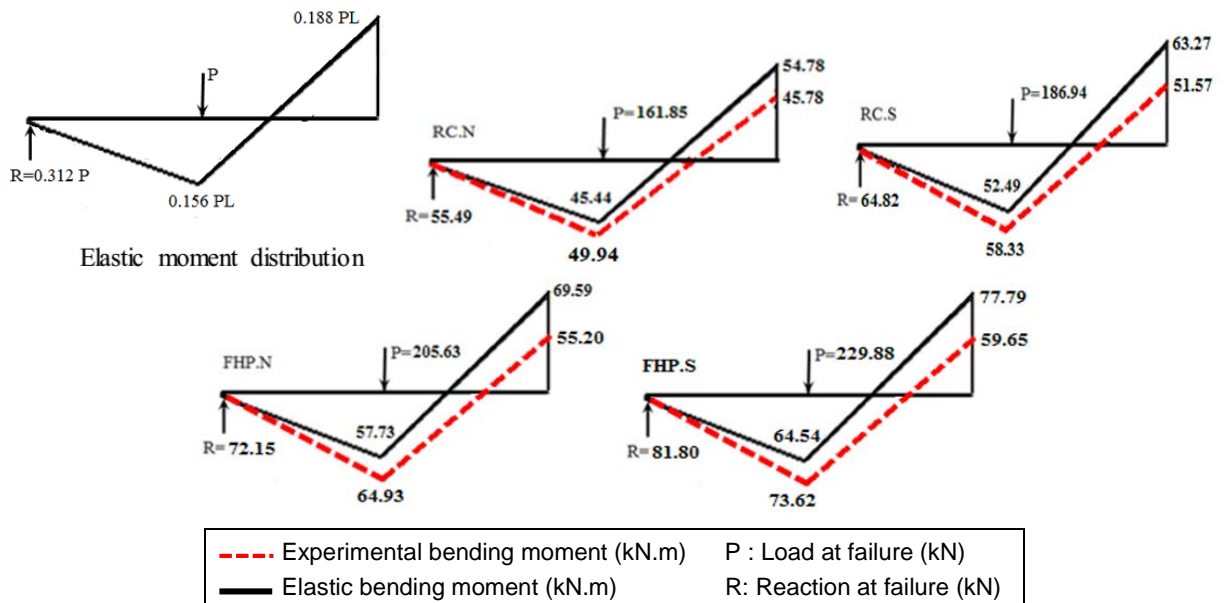


Figure 16. Actual versus elastic bending moment at failure.

4. Conclusion

In this research, the effect of HPFRCC and closed-space stirrups on flexural behavior of two-span reinforced concrete beams was studied and the following important results were concluded:

1. The experimental results showed that using HPFRCC and reducing the spacing of the stirrups and concrete confinement, increased the ultimate load, ductility ratio, energy absorption, plastic hinge characteristics and moment redistribution capacity of these beams compare to reference beam.

2. Comparison of curves of load – displacement of samples of RCN and FHPS showed that the toughness of FHPS improved by 1.82 times more than the RCN. Toughness mechanisms such as bridging the fibers increased tensile strength and reduced the brittle fracture after maximum load.

3. Comparison of the cracking pattern in the plastic zones of the beams showed that the cracking rate in the beams with HPFRCC and closed-space stirrups was more than the RCN beam and As a result, Energy dissipation became more.

4. Unlike beams with regular concrete, in which an initial crack is mostly dominant, HPFRCC beams shows a pseudo-strain hardening behavior with finely distributed multiple cracks. This multiple cracking process occurs in sequence as the applied tensile load increases, after tensile stress reaches the maximum affordable tensile stress of the weakest section, the crack at the weakest section is localized.

5. The displacement ductility and the energy ductility index of FHPS beam was about 1.80 and 1.50 times more than RCN beam respectively.

References

1. Wang, W., Liu, J., Agostini, F., Davy, C.A., Skoczylas, F., Corvez, D. Durability of an Ultra High Performance Fiber Reinforced Concrete (UHPFRC) under progressive aging. *Cement and Concrete Research*. 2014. 55. Pp. 1–13
2. Naaman, A.E. Setting the Stage, Toward Performance Based Classification of FRC Composites. *High Perform Fiber Reinforce Cement Compos (HPFRCC 4)*, Proc 4th Int RILEM Work 2003, 2003.
3. Khatana, S. A review on the use of fibers in reinforced cementitious concrete. *Journal of Industrial Textiles*. 2015. 45(2). Pp. 239–264.
4. Nizina, T.A., Ponomarev, A.N., Balykov, A.S., Pankin, N.A. Fine-grained fibre concretes modified by complexed nanoadditives. *International Journal of Nanotechnology*. 2017. 14(7/8). Pp. 665–679.
5. Nizina, T.A., Balykov, A.S., Volodin, V.V., Korovkin, D.I. Fiber fine-grained concretes with polyfunctional modifying additives. *Magazine of Civil Engineering*. 2017. 72(4). Pp. 73–83. doi: 10.18720/MCE.72.9.
6. Nizina, T.A., Balbalin, A.V. Vliyaniye mineralnykh dobavok na reologicheskie i prochnostnyye arakteristiki cementnykh kompozitov [Influence of mineral additives on the rheological and strength characteristics of cement composites]. *Vestnik TGASU [Bulletin of the Tomsk State University of Architecture and Construction]*. 2012. No. 2. Pp. 148–153. (rus)
7. Nizina, T.A., Balbalin, A.V. 'Mekhanicheskaya aktivatsiya cementnykh smesey spolifunktsionalnymi dobavkami [Mechanical activation of cement mixtures with polyfunctional additives]'. *Regionalnaya arhitektura i stroitelstvo [Regional Architecture and Construction]*. 2013. No. 2. Pp. 36–42. (rus)
8. Selyaev, V.P., Nizina, T.A., Balbalin, A.V. Mnogofunktsionalnye modifikatory cementnykh kompozitov na osnove mine-ralnykh dobavok i polikarboksilatnykh plastifikatorov [Multifunctional modifiers of cement composites based on mineral admixtures and polycarboxylate plasticizers], *Vestnik Volgogradskogo gosudarstvennogo arhitekturnostroitel'nogo uni-versiteta. Seriya: Stroitelstvo i arhitektura [Bulletin of Volgograd State University of architecture and construction. Series: Construction and architecture]*. 2013. No. 31, Part 2. Pp. 156–163. (rus)
9. Rabinovich, F.N. *Dispersno armirovannye betony [Disperse reinforced concretes]*, Stroyizdat, Moscow, 1989. 176 p. (rus)
10. Rabinovich, F.N. *Kompozity na osnove dispersno armirovannykh betonov. Voprosy teorii i proektirovaniya tekhnologiya konstrukcii [Composites based on disperse reinforced concretes. Questions of theory and design, technology, constructions]*. Moscow: Publishing house ASV, 2004. 560 p. (rus)
11. Zagorodnyuk, L.Kh., Shakarna, M., Shchekina, A.Y. Classification of Additives for the Reinforcement of Particulate Composites, GISAP (Global International Scientific Analytical Project), 2013. [Online]. URL: <http://gisap.eu/ru/node/23874>, free, Title from the screen, Language Russian, English.
12. Nizina, T.A., Balykov, A.S. Analiz kompleksnogo vliyaniya modifiziruyushchih dobavok i dispersnogo armirovaniya na fiziko-mekhanicheskie harakteristiki melkozernistykh betonov [Analysis of the combined effect of the modifier additives and particulate reinforcement on the physico-mechanical characteristics of fine-grained concretes]. *Regionalnaya arhitektura i stroitelstvo [Regional Architecture and Construction]*. 2015. No. 4. Pp. 25–33. (rus)
13. Hemmati, A., Kheyroddin, A., Sharbatdar, M.K. Increasing the flexural capacity of RC beams using partially HPFRCC layers. *Comput Concr*. 2015. 16. Pp. 545–568. DOI: <http://dx.doi.org/10.12989/cac.2015.16.4.000>.
14. Hemmati, A., Kheyroddin, A., Sharbatdar, M., Park, Y., Abolmaali, A. Ductile behavior of high performance fiber reinforced cementitious composite (HPFRCC) frames. *Constr Build Mater*. 2016. 115. Pp. 681–9. DOI: 10.1016/j.conbuildmat.2016.04.078.
15. Hemmati, A., Kheyroddin, A., Sharbatdar, M.K. Proposed equations for estimating the flexural characteristics of reinforced HPFRCC beams. *Iran J Sci Technol Trans Civ Eng*. 2014. 38. Pp. 395.
16. Hemmati, A., Kheyroddin, A. and Sharbatdar, M.K. Plastic hinge rotation capacity of reinforced HPFRCC beams. *J. Struct. Eng*. 2014. 141(2). 04014111. DOI: 10.1061/(ASCE)ST.1943-541X.0000858.
17. Akbarzadeh, H., Maghsoudi, A.A. Experimental and analytical investigation of reinforced high strength concrete continuous beams strengthened with fiber reinforced polymer. *Materials and Design*. 2010. 31. Pp. 1130–1147.
18. do Carmo, R., Lopes, S. Required plastic rotation of RC beams. *Proceedings of the Institution of Civil Engineers 2006 structures and Buildings*. 2006. 159(SB3). Pp. 77–86.
19. do Carmo, R., Lopes, S. Ductility and linear analysis with moment redistribution in reinforced high strength concrete beams. *Canadian Journal of Civil Engineering*. 2005a. 32(1). Pp. 194–203. DOI: 10.1139/104-080.

20. do Carmo, R., Lopes, S. Influence of the shear force and transversal reinforcement ratio on plastic rotation capacity Structural Concrete. 2005b. 6(3). Pp. 107–117. DOI: 10.1680/stco.2005.6.3.
21. do Carmo, R. Rotac,ãõ pla'stica e redistribuic,ãõ de esforç,os em vigas de betaõ de alta resistê'ncia "Plastic Rotation and Moment Redistribution in High Strength Concrete Beams"). Ph.D thesis, Universidade de Coimbra, Coimbra, Portugal, 2004. [In Portuguese].
22. Lou, T., Lopes, S.M.R., Lopes, A.V. Evaluation of Moment Redistribution in Normal-Strength and High-Strength Reinforced Concrete Beams. J Struct Eng. 2014. 140. 04014072. DOI: 10.1061/(ASCE)ST.1943-541X.0000994.
23. Iskhakov, I., Ribakov, Y. A design method for two-layer beams consisting of normal and fibered high strength concrete. Mater Des. 2007. 28. Pp. 1672–1677. DOI: 10.1016/j.matdes.2006.03.017.
24. Holschemacher, K., Mueller, T., Ribakov, Y. Effect of steel fibers on mechanical properties of high-strength concrete [Online]. Mater. Des. 2010. 31(5). Pp. 2604–2615. URL: <http://dx.doi.org/10.1016/j.matdes.2009.11.025>.
25. Holschemacher, K., Iskhakov, I., Ribakov, Y., Mueller, T. Laboratory Tests of Two-Layer Beams Consisting of Normal and Fibered High Strength Concrete: Ductility and Technological Aspects. Mech Adv Mater Struct. 2012. 19. Pp. 513–22. DOI: 10.1080/15376494.2011.556840.
26. Mostofinejad, D., Farahbod, F. Parametric study on moment redistribution in continuous RC beams using ductility demand and ductility capacity concept. Iran J Sci Technol. 2007. 31. Pp. 459.
27. Visintin, P., Ali, M.A., Xie, T., Sturm, A.B. Experimental investigation of moment redistribution in ultra-high performance fibre reinforced concrete beams. Construction and Building Materials. 2018. 166. Pp. 433–444.
28. Saghafi, M.h., Shariatmadar, H. Enhancement of seismic performance of beam-column joint connections using high performance fiber reinforced cementitious composites. Construction and Building Materials. 2018. 180. Pp. 665–680.
29. Saghafi, M.h., Shariatmadar, H., Kheyroddin, A. Experimental evaluation of mechanical properties of high performance fiber reinforced cementitious composites. Concr. Res. (JCRE). 2017. 9(2). Pp. 29–42.
30. Bagge, N., O'Connor, A., Elfgrén, L., Pedersen, C. Moment redistribution in RC beams-A study of the influence of longitudinal and transverse reinforcement ratios and concrete strength. Eng Struct. 2014. 80. Pp. 11–23. DOI: [org/10.1016/j.engstruct.2014.08](http://dx.doi.org/10.1016/j.engstruct.2014.08).
31. Bagge, N., O'Connor, A., Pedersen, C. Rotation capacity and plastic redistribution of forces in reinforced concrete beams. Bridge Concr Res Ireland 2012:517–23.
32. American Concrete Institute (ACI). ACI 318M-14: Building Code Requirements for Structural Concrete. 2014.

Contacts:

Ramin Ehsani, 00989121316379; raminehsani1350@gmail.com

Mohammad Sharbatdar, 0098-23-33654070; msharbatdar@semnan.ac.ir

Ali Kheyroddin, 0098-23-33654070; kheyroddin@semnan.ac.ir

© Ehsani, R., Sharbatdar, M.K., Kheyroddin, A., 2019